Dioxygenation of Sterically Hindered (Ethene)Rh^{I} and -Ir^{I} Complexes to (Peroxo)Rh^{III} and (Ethene)(peroxo)Ir^{III} Complexes

Bas de Bruin,*[a] Theo P. J. Peters,[a] Jos B. M. Wilting,[a] Simone Thewissen,[a] Jan M. M. Smits,[a] and Anton W. Gal*[a]

Keywords: Alkene ligands / Iridium / O−O activation / Oxidations / Peroxo ligands

New cationic, five-coordinate bis(ethene)iridium(I) complexes [(κ^3-Me_3-tpa)Ir^{I}(ethene)$_2$]$^+$ (**12**$^+$) and [(κ^3-Me_2-dpa-Me)Ir^{I}(ethene)$_2$]$^+$ (**13**$^+$) have been prepared {Me_3-tpa = *N*,*N*,*N*-tris[(6-methyl-2-pyridyl)methyl]amine, Me_2-dpa-Me = *N*-methyl-*N*,*N*-bis[(6-methyl-2-pyridyl)methyl]amine}. Complexes **12**$^+$ and **13**$^+$ lose one ethene fragment in solution, yielding the five-coordinate mono(ethene) complex [(κ^4-Me_3-tpa)Ir^{I}(ethene)]$^+$ (**14**$^+$) and the four-coordinate mono-(ethene) complex [(κ^3-Me_2-dpa-Me)Ir^{I}(ethene)]$^+$ (**15**$^+$), respectively. [(κ^4-Me_3-tpa)Rh^{I}(ethene)]$^+$ (**11**$^+$), the rhodium analogue of **14**$^+$, was also prepared. Whereas rhodium complex **11**$^+$ is stable in acetonitrile at room temperature, the iridium analogue **14**$^+$ converts to the cyclometallated (acetonitrile)(hydrido) complex **16**$^+$ within 72 h by dissociation of the unique 6-methylpyridyl fragment and oxidative addition of the 6-methylpyridyl C^3–H bond. The four-coordinate mono(-ethene) complex **15**$^+$ is even less stable in solution; it converts to a mixture of compounds within 18 h. Reaction of the mono(ethene)Rh^{I} complex **11**$^+$ with O_2 yields the peroxo complex **17**$^+$ by ethene displacement. In contrast, the mono(-ethene)Ir^{I} complexes **14**$^+$ and **15**$^+$ bind O_2 without the loss of ethene, leading to unprecedented (ethene)(peroxo)Ir^{III} complexes **18**$^+$ and **19**$^+$. At room temperature, peroxo complex **17**$^+$ does not react with ethene and, quite remarkably, C–O bond formation does not occur in the (ethene)(peroxo) complexes **18**$^+$ and **19**$^+$.

Introduction

Mechanistic aspects of oxygenation reactions with environmentally benign dioxygen are poorly understood. In the late transition metal (LTM) catalyzed oxidation of olefins, peroxo and (olefin)peroxo complexes,[1] 3-metalla-1,2-dioxolanes,[1,2] and 2-metallaoxetanes[3,4] have been proposed as crucial intermediates. In an attempt to collect more mechanistic insight in LTM-mediated oxygenation of olefins we are investigating the stoichiometric oxygenation of rhodium(I)- and iridium(I)-coordinated olefins by O_2.

We have previously observed the selective oxygenation of the cationic (ethene)Rh^{I} and -Ir^{I} complexes **1**$^+$−**4**$^+$ by H_2O_2 *in solution* (various solvents), to give 2-rhoda(III)- and 2-irida(III)oxetanes (1-oxa-2-metalla(III)cyclobutanes) **5**$^+$−**8**$^+$ (Scheme 1).[5,6] Recently, we also observed monooxygenation of cationic (ethene)Ir^{I} complexes by O_2; reaction of **4**$^+$ with air or O_2 in CH_2Cl_2 led to formation of approximately 25% of **8**$^+$.[6]

Furthermore we observed slow, selective dioxygenation of *solid* **1** with air or O_2 to the 3-metalla-1,2-dioxolanes **9a**$^+$ and **9b**$^+$. The ratio between these geometrical isomers proved to be counterion-dependent.[7] Recently, we observed a similar reaction for the iridium analogue **3**$^+$ yielding **10a**$^+$ and **10b**$^+$.[8]

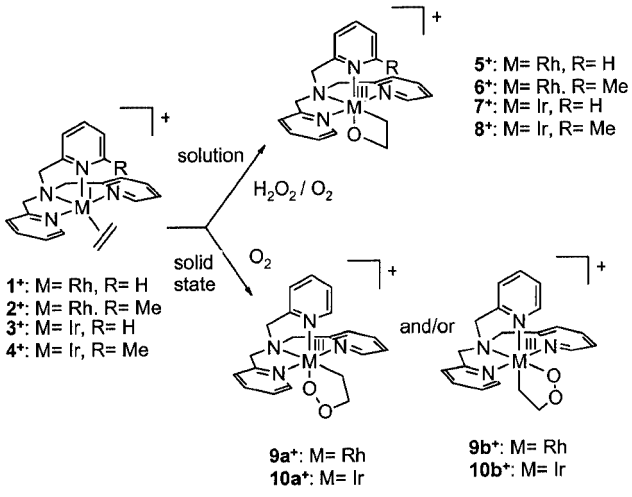

Scheme 1. Mono- and dioxygenation of (ethene)Rh^{I} and -Ir^{I} complexes by O_2

In order to improve our understanding of the mechanisms by which the above reactions proceed, we have now studied the reactivity of [(ethene)(N-ligand)M^{I}]$^+$ (M = Rh, Ir) complexes containing the more bulky N-ligands Me_3-tpa and Me_2-dpa-Me.

[a] Department of Inorganic Chemistry, University of Nijmegen, Toernooiveld 1, 6525 ED Nijmegen, The Netherlands
Fax: (internat.) + 31-24/355-34 50
E-mail: BdeBruin@sci.kun.nl
gal@sci.kun.nl

Results and Discussion

1. Synthesis of (Ethene)Rh^{I} and -Ir^{I} Complexes

We synthesized the cationic ethene complex [(Me_3TPA)-$Rh^{I}(C_2H_4)]^+$ (**11**$^+$) using the route in Scheme 2. Stirring of $[\{(C_2H_4)_2Rh^{I}(\mu\text{-Cl})\}_2]$ with Me_3-tpa in MeOH at −78 °C resulted in the formation of **11**$^+$, which was isolated as [**11**]PF_6 by precipitation with KPF_6.

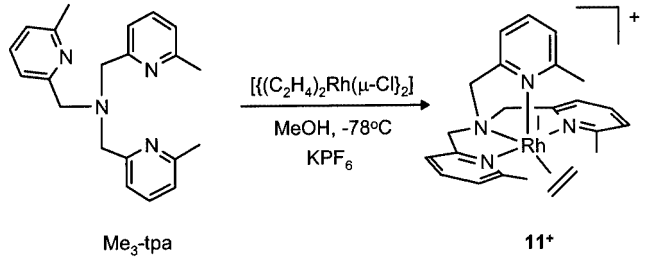

Scheme 2. Preparation of (ethene)Rh^{I} complex **11**$^+$

A similar reaction of $[(C_2H_4)_4Ir^{I}(Cl)]$[9] (generated in situ from the reaction of $[\{(coe)_2Ir^{I}(\mu\text{-Cl})\}_2]$[10] with ethene; coe = cyclooctene) in MeOH with Me_3-tpa and Me_2-dpa-Me yielded the bis(ethene)iridium complexes [(Me_3-tpa)$Ir^{I}(C_2H_4)_2]^+$ (**12**$^+$) and [(Me_2-dpa-Me)$Ir^{I}(C_2H_4)_2]^+$ (**13**$^+$), respectively (Scheme 3). The cations **12**$^+$ and **13**$^+$ were isolated as PF_6^- salts by precipitation with KPF_6.

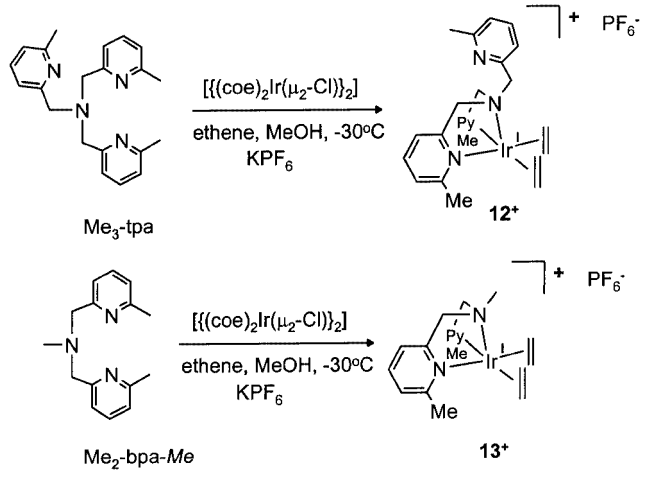

Scheme 3. Synthesis of bis(ethene)Ir^{I} complexes **12**$^+$ and **13**$^+$

The ^1H and ^{13}C NMR spectroscopic data of **12**$^+$ and **13**$^+$ reveal two equivalent N-CH_2-Py^{Me} groups. The ^1H NMR methyl signals of these two groups have shifted by approximately 0.7 ppm downfield relative to the free ligand, in both **12**$^+$ and **13**$^+$. As expected, the diastereotopic methylene protons of the two equivalent N-CH_2-Py^{Me} groups give rise to two AB-type doublets. The ^1H NMR methyl signal of the unique N-CH_2-Py^{Me} group of **12**$^+$ at δ = 2.6 ppm is close to the value of that of the free ligand (δ = 2.56 ppm). In the ^1H NMR spectra of **12**$^+$ and **13**$^+$, the ethene fragments are observed as two broad signals between δ = 2.1 and 1.6 ppm at room temperature.

The X-ray structure of **12**$^+$ was determined. Despite of the poor quality of the data set obtained, the X-ray analysis clearly shows the presence of the κ^3-*N,N,N-fac*-coordinated Me_3-tpa ligand with a noncoordinated 6-methylpyridyl group. The structure is in good agreement with the NMR spectroscopic data in solution (Figure 1).

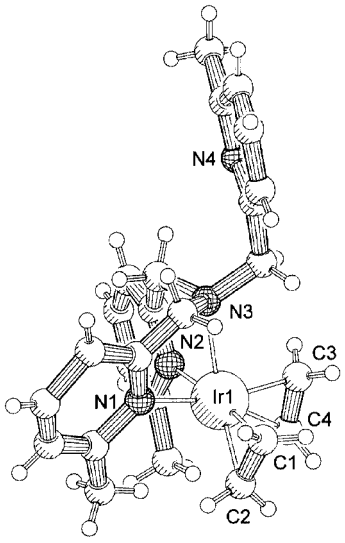

Figure 1. X-ray structure of **12**$^+$

The coordination mode of **12**$^+$ is best described as pseudo square-pyramidal (sqpy). Analogously, complex **13**$^+$ will most probably be square-pyramidal, too.

2. Ethene Dissociation from Bis(ethene)Ir^{I}

Solutions of the bis(ethene) complexes **12**$^+$ and **13**$^+$ are not stable. One of the two ethene fragments dissociates in [D_6]acetone, CD_2Cl_2, or MeCN within 4 h at room temperature (Scheme 4). For **12**$^+$, substitution of the ethene fragment by the unique 6-methylpyridyl group results in the mono(ethene) complex [(κ^4-Me_3-tpa)Ir^{I}(ethene)]$^+$ (**14**$^+$), which is the iridium analogue of **11**$^+$. Ethene dissociation from **13**$^+$ results in the four-coordinate mono(ethene) complex **15**$^+$.

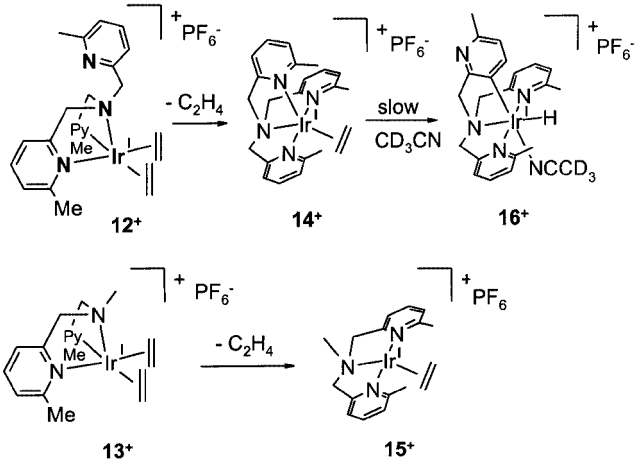

Scheme 4. Ethene dissociation from bis(ethene)Ir^{I} complexes **12**$^+$ and **13**$^+$ resulting in the mono(ethene) complexes **14**$^+$ and **15**$^+$ and the cyclometallated complex **16**$^+$

At room temperature the ^{1}H and ^{13}C NMR spectra of **14^{+}** show two equivalent and one unique N-CH_2-Py^{Me} fragment, consistent with a κ^4-coordination mode of the Me_3-tpa ligand. The ^{1}H and ^{13}C NMR spectra of **15^{+}** show signals for two equivalent N-CH_2-Py^{Me} groups. The ethene signals of both **14^{+}** and **15^{+}** are observed as two sharp triplets, indicating that the ethene fragment does not rotate on the NMR time scale.

The ^{1}H NOE patterns of **15^{+}** are characteristic of a *mer*-coordination mode of the Me_2-dpa-Me ligand; clear NOE contacts are observed between N-*CH_3* and the equatorial N-*CH_2*-Py^{Me} methylene protons (one of the two AB-type doublets). The latter also show NOE contacts with the Py-H^3 protons. The axial N-*CH_2*-Py^{Me} methylene protons (the other AB-type doublet) do not show NOE contacts with either N-*CH_3* or Py^{Me}-*H^3*.

The mono(ethene) complexes **14^{+}** and **15^{+}** are only moderately stable at room temperature, in solution. Complex **14^{+}** is in marked contrast with the less substituted tpa and (Me-tpa)Ir^{I}(ethene) complexes **3^{+}** and **4^{+}**, which are stable in solution over a period of days. Complex **15^{+}** decomposes in CD_2Cl_2 or CD_3CN to a complex mixture of products within 18 h. In CD_3CN, complex **14^{+}** selectively converts in 72 h to cyclometallated complex **16^{+}**, presumably by chelate ring opening, oxidative addition of the 6-methylpyridyl C^3−H bond to the Ir^{I} center and substitution of ethene by CD_3CN (Scheme 4). The hydride in **16^{+}** is observed as a sharp ^{1}H NMR signal at $\delta = -18.6$ ppm. The presence of a coordinated CD_3CN was confirmed by ESI-MS and elemental analysis. The observed cyclometallation also occurs in acetone or CH_2Cl_2. In these solvents, however, ^{1}H NMR spectroscopy indicates that the 6th coordination site is still occupied by ethene.

A solution of **15^{+}** in CD_2Cl_2 contains only **15^{+}**. In CD_3CN, however, **15^{+}** and **15^{+}**(CD_3CN) are present in a ratio of 3:1. Although they have separate ^{1}H NMR signals, they show exchange signals in the EXSY spectrum, indicating that **15^{+}** and **15^{+}**(CD_3CN) are in slow exchange on the ^{1}H NMR time scale. The ethene ^{1}H NMR signals of **15^{+}**(CD_3CN) are very similar to those of **14^{+}**. The ethene signals of **15^{+}**, both in CD_3CN and CD_2Cl_2, have clearly shifted downfield relative to those of **14^{+}**. Computer-generated space-filling models of **15^{+}** indicate that the methyl substituents on the pyridyl fragments must hinder a true square-planar coordination geometry (see also Figure 4 and the discussion of the structure of complex **19^{+}**). Therefore, we propose that **15^{+}** has a distorted square-planar geometry, in which the ethene fragment has moved to a position below the *mer*-(Me-dpa-Me)Ir plane, away from the N_{amine}-Me and the Py-6-Me substituents (Scheme 4). From MO calculations it is known that such a distortion towards a mono-vacant trigonal-bipyramidal coordination geometry increases the reactivity of d^8-metal centers towards oxidative addition of a C−H bond.[11] This could explain the apparent reactivity of **15^{+}** in solution at room temperature. Dissociation of the unique 6-methyl-pyridyl fragment of **14^{+}** would lead to a similar distorted square-planar geometry, thus accounting for its intramolecular C−H activation.

3. Electrochemical Oxidation of the (Ethene)Rh^{I} and -Ir^{I} Complexes

The electrochemical oxidation of the ethene complexes **11^{+}**−**15^{+}** (Schemes 2 and 3) was studied by means of cyclic voltammetry. Table 1 summarizes the electrochemical data.

Table 1. Electrochemical data for complexes **11^{+}**−**15^{+}** [measured in MeCN (0.1 M TBAH); potentials in mV vs. the Fc/Fc^{+} couple]

	M	E^{p}_{anode}	$E^{p}_{cathode}$	$E_{1/2}$	I_b/I_f	ΔE
12^{+}	Ir	188	57	124[a]	0.53	114
13^{+}	Ir	156	90	123	1.00	66
11^{+}	Rh	−272	−426	−349[a]	0.48	154
14^{+}	Ir	−330	−399	−365	1.00	69
15^{+}/15^{+}(MeCN)	Ir	−226	−	−	0.00	−

[a] Quasi-reversible.

Clearly, the mono(ethene) complexes **11^{+}**, **14^{+}**, and **15^{+}**/**15^{+}**(MeCN) are oxidized at much lower potentials (−226 to −330 mV vs. Fc/Fc^{+}) than the bis(ethene) complexes **12^{+}** and **13^{+}** (+156 to +188 V vs. Fc/Fc^{+}). This presumably stems from an increased electron density at the metal center (due to decreased π-back donation) as a result of the loss of one ethene fragment. As expected, the (N_4-ligand)-Rh^{I} complex **11^{+}** is oxidized at a higher potential than the (N_4-ligand)Ir^{I} complex **14^{+}**.

The five-coordinate bis- and mono(ethene)Ir^{I} complexes **13^{+}** and **14^{+}** (Scheme 4) undergo reversible one-electron oxidation at 100 mV/s in MeCN (0.1 M TBAH). The five-coordinate mono(ethene)Rh^{I} complex **11^{+}** and bis(ethene)Ir^{I} complex **12^{+}** both undergo quasi-reversible one-electron oxidation. In contrast, the mono(ethene) complex **15^{+}**/**15^{+}**(MeCN) is oxidized irreversibly in MeCN at 100mV/s.

During conversion of the bis(ethene) complexes **12^{+}** and **13^{+}** to the mono(ethene) complexes **14^{+}** and **15^{+}**, respectively, the redox pairs **12^{+}**/**14^{+}** and **13^{+}**/**15^{+}** are both seen as separate waves in the cyclic voltammogram. Therefore the bis(ethene) complexes are not in equilibrium with the mono(ethene) complexes on the electrochemical time scale.

4. Oxidation of the (Olefin)Rh^{I} and -Ir^{I} Complexes by O_2

The reactivity of the (ethene)rhodium complex **11^{+}** and the (ethene)iridium complexes **12^{+}**−**15^{+}** towards O_2 has been investigated. For the rhodium complex **11^{+}**, we observed clean ethene displacement by O_2. In contrast, the iridium complexes **14^{+}** and **15^{+}** react aselectively. For 25% the complexation of O_2 occurs without dissociation of ethene, giving **18^{+}** and **19^{+}** (Scheme 5).

Treatment of a CD_2Cl_2 solution of the Rh^{I} complex **11^{+}** with O_2 resulted in selective formation of the (peroxo)Rh^{III} complex **17^{+}**, according to ^{1}H NMR spectroscopy and ESI-MS. Loss of ethene was confirmed by ^{1}H NMR spectroscopy. The ^{1}H and ^{13}C NMR spectroscopic data of **11^{+}**, showing two equivalent and one unique N-CH_2-Py^{Me} frag-

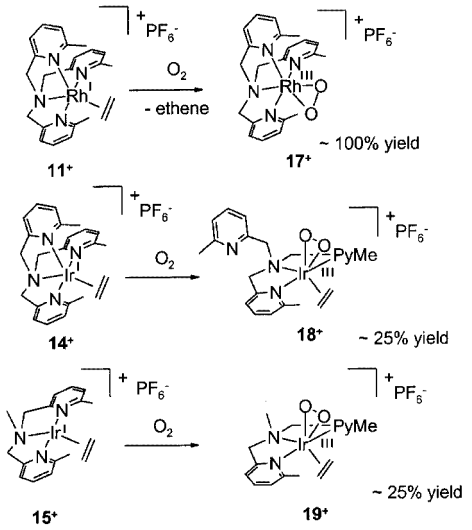

Scheme 5. Reaction of (ethene)Rh^{I} and -Ir^{I} complexes to (peroxo)Rh^{III} and (ethene)(peroxo)Ir^{III} complexes

ment, are in accordance with a κ^4-coordination mode of the Me_3TPA ligand. ^{1}H NMR and ESI-MS indicate that the reaction of [(Me_2-tpa)Rh^{I}(ethene)]$^+$ with O_2 also results in selective formation of the (peroxo)Rh^{III} complex [(Me_2-tpa)$Rh^{II}(O_2)$]$^+$. In solution, Me_x-tpa complexes with less Me substituents, viz. [(Me_x-tpa)Rh^{I}(ethene)]$^+$ (x = 0, 1) lose ethene upon contact with O_2 or air in an aselective reaction.

Upon reaction of (mono)etheneIr^{I} complex **14**$^+$ with 1.2 bar O_2 in CD_2Cl_2, the ^{1}H NMR spectrum showed intense signals from the (ethene)(peroxo) complex **18**$^+$ and very broad signals, probably from paramagnetic species (Scheme 5). Based on the intensity of the ^{1}H NMR signals of **18**$^+$ relative to the internal standard dichloroethane, the starting complex **14**$^+$ has been converted into **18**$^+$ for approximately 25%, and approximately 70% of (a) paramagnetic compound(s). The reaction of complex **15**$^+$ with 1.2 bar O_2 in CD_2Cl_2 proceeds similarly to that of **14**$^+$. Again, approximately 25% of the (ethene)(peroxo) complex **19**$^+$ and approximately 70% of unidentified paramagnetic species are formed (Scheme 5). Any attempts to improve the selectivity of these reactions, e.g. by treatment of [**14**]PF_6 or [**15**]PF_6 with only 1 equiv. O_2 or by performing the reactions at lower temperatures, were not successful. Nevertheless, we succeeded in the isolation of pure [**18**]PF_6 and [**19**]PF_6 through crystallization.

The ^{1}H and ^{13}C NMR spectra of **18**$^+$ and **19**$^+$ show signals for two equivalent N-CH_2-Py^{Me} groups. The equatorial N−CH_2−Py^{Me} group of **18**$^+$ gives rise to a ^{1}H NMR methyl signal at δ = 2.65 ppm, close to the value for the free ligand (δ = 2.56 ppm). The methyl signals of the two equivalent 6-methylpyridyl groups of **18**$^+$ and **19**$^+$ are approximately 0.4 ppm downfield from those in the free ligand. The diastereotopic methylene protons of the two equivalent N-CH_2-Py^{Me} groups give rise to two AB-type doublets.

On going from (ethene)Ir^{I} compounds **14**$^+$ and **15**$^+$ to the (ethene)(peroxo)Ir^{III} species **18**$^+$ and **19**$^+$ the rate of ethene rotation increases. In the 200 MHz ^{1}H NMR spectra of **18**$^+$ and **19**$^+$ at room temperature, the ethene fragments are observed as very broad signals at δ = 4.48 and 4.22 ppm, respectively. At 500 MHz, the broad signals have split into two sharp triplets at 233 K for both **18**$^+$ (δ = 4.84 and 4.14 ppm, $^3J_{H,H}$ = 9.70 Hz) and **19**$^+$ (δ = 4.56 and 3.77 ppm, $^3J_{H,H}$ = 9.40 Hz). For both **18**$^+$ and **19**$^+$, at 500 MHz, coalescence of these triplets into one signal occurs at T_c = 273 K. From these data, the free energy of activation ($\Delta G_c^{\neq}$) for ethene rotation in **18**$^+$ and **19**$^+$ at T_c was estimated to be ca. 12 kcal/mol. The ethene fragments of **14**$^+$ and **15**$^+$ do not rotate on the ^{1}H NMR time scale at room temperature (298 K, 200 MHz). The free energy of activation for ethene rotation ($\Delta G_c^{\neq}$) of **14**$^+$ and **15**$^+$, as estimated from line-width analysis of the ethene ^{1}H NMR signals, must be at least 17 kcal/mol.

The structures of [**18**]PF_6 (Figure 2) and [**19**]PF_6 (Figure 3) were determined by single-crystal X-ray diffraction.

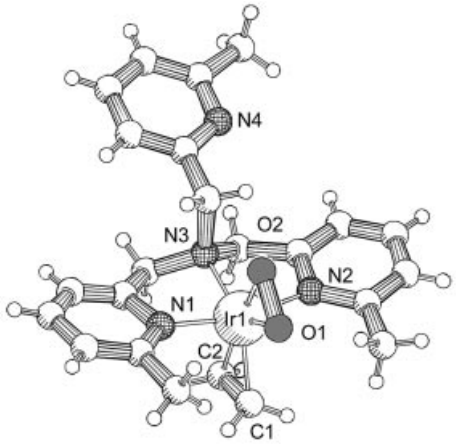

Figure 2. X-ray structure of **18**$^+$; selected bond lengths [Å] and angles [°]: Ir1−N1 2.071(12), Ir1−N2 2.085(12), Ir1−N3 2.073(11), Ir1−O1 2.014(10), Ir1−O2 2.011(9), Ir1−C1 2.119(14), Ir1−C2 2.162(14), O1−O2 1.430(13), C1−C2 1.40(2); N1−Ir1−N2 162.3(5), N1−Ir1−N3 80.7(5), N2−Ir1−N3 81.6(5), O1−Ir1−N3 136.7(4), O2−Ir1−N3 95.1(4), C1−Ir1−N3 128.4(5), C2−Ir1−N3 90.1(5), O1−Ir1−C1 94.9(5), O1−Ir1−C2 133.1(5), O2−Ir1−C1 136.5(5), O2−Ir1−C2 174.6(5)

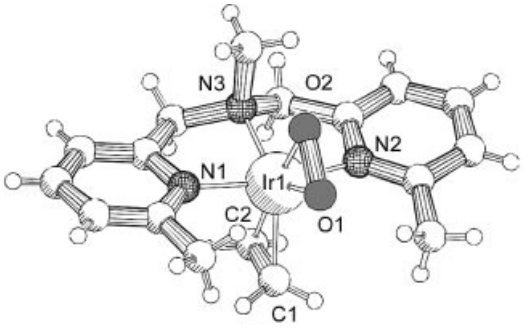

Figure 3. X-ray structure of **19**$^+$; selected bond lengths [Å] and angles [°]: Ir1−N1 2.083(6), Ir1−N2 2.076(5), Ir1−N3 2.098(5), Ir1−O1 2.046(5), Ir1−O2 2.023(5), Ir1−C1 2.122(7), Ir1−C2 2.136(7), O1−O2 1.446(8), C1−C2 1.404(11); N1−Ir1−N2 164.0(2), N1−Ir1−N3 81.5(2), N2−Ir1−N3 82.7(2), O1−Ir1−N3 136.0(2), O2−Ir1−N3 94.4(2), C1−Ir1−N3 127.1(3), C2−Ir1−N3 88.8(3), O1−Ir1−C1 96.8(3), O1−Ir1−C2 135.1(3), O2−Ir1−C1 138.4(3), O2−Ir1−C2 176.1(5)

The X-ray structure of **18**$^{+}$ reveals a κ^3-*mer*-coordinated Me_3-tpa ligand with a noncoordinated 6-methylpyridyl group, in accordance with the NMR spectroscopic data. Thus, dissociation of the unique pyridyl group probably precedes the reaction of **14**$^{+}$ with O_2. It is therefore not surprising that the reaction of **15**$^{+}$ with O_2 proceeds similarly.

The O−O distances in **18**$^{+}$ [1.430(13) Å] and **19**$^{+}$ [1.446(8) Å] indicate that the coordinated η^2-O_2 is best described as an η^2-peroxo fragment. Consequently the iridium center is formally in the +III oxidation state. The Ir−C and C−C distances for coordinated ethene in **18**$^{+}$ and **19**$^{+}$, however, fit well within the Ir−C and C−C ranges reported for (ethene)Ir^{I} complexes (ranges found in the Cambridge Structural Database: Ir^{I}−C: 2.036−2.191 Å, C−C: 1.351−1.444 Å).

Viewing the stick representation of (ethene)(peroxo) complex **19**$^{+}$ along the N1−Ir1−N2 axis reveals that folding of Me_2-dpa-Me to its *mer*-coordination mode leaves a relatively small compartment for *cis* coordination to the N3-Me fragment and a relatively large compartment for *trans* coordination to the N3-Me fragment (*cis* and *trans* with respect to the Ir1−N3 axis, Figure 4).

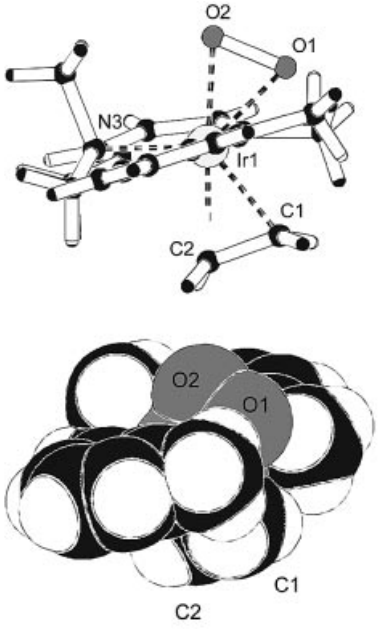

Figure 4. X-ray structure of **19**$^{+}$; top: stick representation; bottom: CPK representation

Viewing the CPK representation of **19**$^{+}$ (Figure 4, right) suggests that *mer*-Me_2-dpa-Me in the ethene complex **15**$^{+}$ allows ethene coordination neither in the small *cis* compartment (resulting in a mono-vacant trigonal-bipyramidal geometry) nor at a position *trans* to N3, in between the Py-Me groups (resulting in a square-planar geometry). It is therefore tempting to assume that **15**$^{+}$ (Scheme 4) has a mono-vacant trigonal-bipyramidal coordination geometry, with ethene coordinated *trans* to the N3-Me fragment, close to the structure of **19**$^{+}$ without the peroxo fragment. Binding of O_2 to **15**$^{+}$ would thus involve only small structural rearrangements.

5. π-Back Bonding in (Ethene)Rh^{I}, -Ir^{I} and -Ir^{III} Complexes

The ethene signals of four-coordinate **15**$^{+}$ have shifted down-field relative to those of five-coordinate **14**$^{+}$, both in ^{1}H NMR (**15**$^{+}$: δ = 3.54 and 2.34 ppm; **14**$^{+}$: δ = 1.85 and 1.37 ppm) and ^{13}C NMR (**15**$^{+}$: δ = 37.0 and 25.1 ppm; **14**$^{+}$: δ = 3.7 and 0.2 ppm). The ethene signals of the five-coordinate Rh^{I} complex **11**$^{+}$ (^{1}H NMR: δ = 2.41 and 2.11 ppm; ^{13}C NMR: δ = 29.5 and 26.3 ppm) have also shifted down-field relative to those of its Ir^{I} analogue **14**$^{+}$. Furthermore, the (N_4-ligand)Rh^{I} complex **11**$^{+}$ is oxidized at a potential 60 mV higher than that of the (N_4-ligand)Ir^{I} complex **14**$^{+}$. These data are consistent with weaker M→C=C π-back donation upon removal of a donor atom (from **14**$^{+}$ to **15**$^{+}$) and upon substitution of rhodium(I) for iridium(I) (from **14**$^{+}$ with **11**$^{+}$).

The increased rate of ethene rotation on going from (ethene)Ir^{I} compounds **14**$^{+}$ and **15**$^{+}$ to (ethene)(peroxo)Ir^{III} species **18**$^{+}$ and **19**$^{+}$ (vide infra) most likely results from decreased Ir→C=C π-back bonding for Ir^{III} relative to Ir^{I}.

Discussion and Conclusions

Complexes **18**$^{+}$ and **19**$^{+}$ are very rare examples of (olefin)(peroxo) complexes. In the only other structurally characterized (peroxo)(olefin)transition-metal complex **20**, the olefin fragment is part of the stabilizing P-ligand (Figure 5).[12] Olefin coordination in **20** must be promoted by the chelate effect, in contrast to ethene coordination in **18**$^{+}$ and **19**$^{+}$.

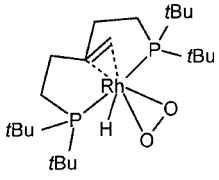

20

Figure 5. (Olefin)(peroxo)rhodium complex **20**[12]

For **18**$^{+}$, **19**$^{+}$, and **20** it is quite remarkable that the olefin fragment does not insert into the M−O bond of the η^2-peroxo fragment. The approach of the peroxo fragment by the olefin fragment might be hindered by geometrical constraints, i.e. the fixed position of the olefin in the rigid chelating diphosphane ligand in **20** and for steric reasons in **18**$^{+}$ and **19**$^{+}$. However, there seems to be no obvious geometrical constraint for the peroxo fragment to move towards the olefin. Nevertheless, intramolecular C−O bond formation is not observed.

The (peroxo)Rh^{III} complex **17**$^{+}$ and the unprecedented (ethene)(peroxo)Ir^{III} complexes **18**$^{+}$ and **19**$^{+}$ add to the list of species observed upon reaction of [(N-ligand)M^{I}(ethene)]$^{+}$ (M = Rh, Ir) with O_2 (**a** and **b** in

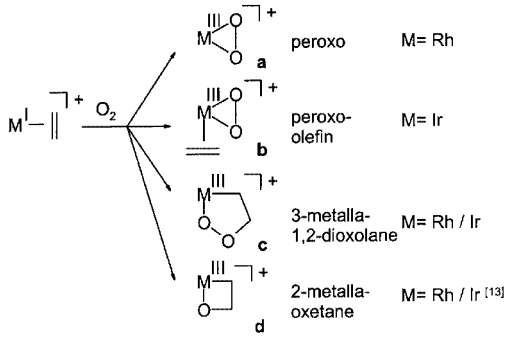

Scheme 6. Observed oxygenations of $[(\text{N-ligand})\text{M}^{\text{I}}(\text{olefin})]^+$ (M = Rh, Ir) by O_2

Scheme 6). The reactivity of (ethene)Rh^{I} and -Ir^{I} fragments towards dioxygen thus varies from ethene displacement (**a**) and formation of mixed (ethene)(O_2) complexes (**b**) to C−O bond formation (to give a 3-metalla-1,2-dioxolane; **c**) and to C−O bond formation plus O−O bond breaking (to give a 2-metallaoxetane; **d**).[13] Apparently, the outcome of the oxygenation reaction subtly depends on the metal and the N-ligand (Scheme 6).

The remarkable effects of variation of metal and N-ligand on the obtained products are best demonstrated by comparing **11**$^+$ (Scheme 5), **14**$^+$ (Scheme 5), and **4**$^+$ (Scheme 1) in their solution-phase reactivity towards O_2. Changing the metal from rhodium in **11**$^+$ to iridium in **14**$^+$ results in (η^2-ethene)(η^2-peroxo) complex **18**$^+$ instead of η^2-peroxo complex **17**$^+$. Apparently ethene binds stronger to iridium(III) than to rhodium(III).[14] Changing the ligand from Me_3-tpa in **14**$^+$ to Me-tpa in **4**$^+$ results in 2-iridaoxetane **8**$^+$, instead of the (ethene)(peroxo) complex **18**$^+$, as the observed product.

One could imagine peroxo species of type **a** (analogues of **17**; Scheme 5) to react with olefins, yielding 3-metalla-1,2-dioxolanes **c** (analogues of **9**$^+$ or **10**$^+$; Scheme 1) or 2-metallaoxetanes **d** (analogues of **1**−**4**; Scheme 1). Insertion of ethene into the Ir−O bond of (ethene)(peroxo) complexes **b** (analogues of **18**$^+$ or **19**$^+$; Scheme 5) would seem a simple and viable route to 3-metalla-1,2-dioxalanes **c**. However, at room temperature, the (peroxo)Rh^{III} species **17**$^+$ shows no further reactivity towards ethene, and the (ethene)(peroxo)Ir^{III} complexes **18**$^+$ and **19**$^+$ do not undergo insertion of ethene into the Ir−O bond. The 3-metalla-1,2-dioxolane isomers **9**$^+$ and **10**$^+$ (Scheme 1) are only formed from **1**$^+$ and **3**$^+$ in the *solid state*, whereas *in solution* very aselective reactions yield other products without any indication for the formation of **9**$^+$ or **10**$^+$. It is hard to believe that chelate ring opening, which would be required to form a (ethene)(peroxo) complex analogous to **18**$^+$, plays a role in the *solid state* reactions. Therefore, 3-metalla-1,2-dioxolanes **c** probably form by alternative routes in the *solid state*.

In **14**$^+$, relieving the steric strain by the Me substituents in the κ^4-coordination mode of the Me_3-tpa ligand through dissociation of a 6-methylpyridyl fragment apparently opens up the "κ^3-route" to the formation of **18**$^+$. As such strain is absent in the Me-tpa complex **4**$^+$, formation of 2-iridaoxetane **8**$^+$ might proceed by a "κ^4-route". However, we cannot exclude that the formation of the (ethene)-(peroxo) complex **18**$^+$, instead of an analogue of 2-iridaoxetane **8**$^+$ (Scheme 1), merely reflects a thermodynamic preference, resulting from the weaker N-donor capacity of the Me_3-tpa ligand.

Experimental Section

General Methods: All procedures were performed under N_2 using standard schlenk techniques unless otherwise indicated. Solvents (p.a.) were deoxygenated by bubbling a stream of N_2 through the solvent or by the freeze-pump-thaw method. Room temperature corresponds to ca. 20 °C. NMR spectroscopic experiments were carried out with a Bruker DPX200 (200 MHz and 50 MHz for ^{1}H and ^{13}C, respectively), a Bruker AC300 (300 MHz and 75 MHz for ^{1}H and ^{13}C, respectively), a Varian Inova 400 (400 MHz and 100 MHz for ^{1}H and ^{13}C, respectively) and a Bruker AM500 (500 MHz and 125 MHz for ^{1}H and ^{13}C, respectively). Solvent shift reference for ^{1}H NMR spectroscopy: [D_6]acetone δ_H = 2.05, CD_3CN δ_H = 1.94, CD_2Cl_2 δ_H = 5.31. For ^{13}C NMR: [D_6]acetone δ_C = 29.50, CD_3CN δ_C = 1.25, CD_2Cl_2 δ_C = 54.20. Abbreviations used are s = singlet, d = doublet, dd = doublet of doublets, t = triplet, dt= doublet of triplets, q = quadruplet, dq = doublet of quadruplets, m = multiplet and br = broad. Py^A represents the two equivalent 6-methylpyridyl groups, Py^B represents the unique 6-methylpyridyl group. Elemental analyses (C,H,N) were carried out with a Carlo Erba NCSO analyzer. Mass spectra (FAB, ESI) were recorded with a MAT 900 XL mass spectrometer or a JEOL JMS SX/SX102A four-sector mass spectrometer. Cyclic voltammetry measurements were performed using an Eco Chemie Autolab PGSTAT20. A conventional three-electrode cell, with Pt working and auxiliary electrodes and 0.1 M [(nBu)$_4$N]PF_6 (TBAH) electrolyte was used. An Ag/AgI reference electrode (grain of AgI, 0.02 M [(nBu)$_4$N]I (TBAI) and 0.1 M TBAH) was employed. Me_3-tpa,[15] [{(C_2H_4)$_2$Rh(μ-Cl)}$_2$],[16] and [{(coe)$_2$Ir(μ-Cl)}$_2$][10] were prepared according to literature procedures. All other chemicals were commercially available and were used without further purification, unless otherwise stated.

X-ray Diffraction: Single crystals were mounted in air on glass fibers. Intensity data were collected at room temperature. An Enraf−Nonius CAD4 single-crystal diffractometer was used, applying graphite-monochromatized Cu-K_α or Mo-K_α radiation. Unit cell dimensions were determined from the angular setting of 22 reflections for [**12**]PF_6, 24 reflections for [**18**]PF_6 and 25 reflections for [**19**]PF_6. Intensity data were corrected for Lorentz and polarization effects. Semiempirical absorption correction (ψ-scan) was applied for all compounds.[17] The structures were solved by the program system DIRDIF[18] using the program PATTY[19] to locate the heavy atoms. All structures were refined with standard methods (refinement against F^2 of all reflections with SHELXL-97[20]) with anisotropic parameters for the non-hydrogen atoms. Hydrogen atoms were placed at calculated positions and were subsequently refined isotropically in riding mode. For [**18**]PF_6 and [**19**]PF_6 geometrical data with regard to O1, O2, C1, and C2 are rather similar. The assignment of atomic species has been made on the basis of prior occupancy factor refinement and comparison of thermal displacement parameters. Selected bond lengths and angles are summarized in Figures 1−3. Drawings were generated with the program PLATON.[21] Other relevant crystal data are summarized in Table 2. Crystallographic data (excluding structure factors) for the

Table 2. Crystallographic data for [**12**]PF_6, [**18**]PF_6, and [**19**]PF_6

	[**12**]PF_6·CH_3OH·1/2H_2O	[**18**]PF_6·1/2H_2O	[**19**]PF_6
Empirical formula	$C_{25.5}H_{36}F_6IrN_4O_{1.5}P$	$C_{23}H_{29}F_6IrN_4O_{2.5}P$	$C_{17}H_{23}F_6IrN_3O_2P$
Formula mass	759.75	738.67	638.55
Crystal size [mm]	0.63 × 0.28 × 0.13	0.36 × 0.11 × 0.10	0.52 × 0.38 × 0.20
T [K]	293(2)	293(2)	293(2)
Crystal system	orthorhombic	monoclinic	triclinic
Space group	*Pbcn*	$P2_1/c$	$P\bar{1}$
a [Å]	31.9939(19)	9.583(2)	7.001(3)
b [Å]	12.1203(8)	24.768(5)	12.081(4)
c [Å]	14.7332(8)	12.0374(13)	12.414(3)
α [°]	90	90	90.91(2)
β [°]	90	100.420(12)	90.74(2)
γ [°]	90	90	100.699(17)
V [Å^3]	5713.2(6)	2809.8(9)	1031.5(6)
$\rho_{calcd.}$ [gcm^{-3}]	1.767	1.746	2.056
Z	8	4	2
Diffractometer	Enraf−Nonius CAD4	Enraf−Nonius CAD4	Enraf−Nonius CAD4
Scan	ω-scan	ω-scan	ω/2θ-scan
Radiation	Cu-K_α	Mo-K_α	Mo-K_α
Wavelength [Å]	1.54184	0.71073	0.71073
F(000)	3000	1444	616
θ range [°]	3.90−54.96	3.11−27.49	2.96−27.48
Index ranges	$-33 \le h \le 0$	$-12 \le h \le 12$	$0 \le h \le 9$
	$-12 \le k \le 0$	$0 \le k \le 32$	$-15 \le k \le 15$
	$-15 \le l \le 0$	$0 \le l \le 15$	$-16 \le l \le 16$
Measured reflections	3586	6705	5112
Unique reflections	3586	6408	4724
Observed refl. [$I_o > 2\sigma(I_o)$]	1688	2563	4273
Refined parameters	357	337	274
Goodness-of-fit on F^2	1.110	0.907	1.142
R [$I_o > 2\sigma(I_o)$]	0.0844	0.0784	0.0423
$wR2$ (all data)	0.2202	0.1808	0.1111
ρ_{fin} (max/min) [e·Å^{-3}]	1.017/−0.891	0.784/−0.785	2.889/−3.954

structures reported in this paper have been deposited with the Cambridge Crystallographic Data Centre as supplementary publication no. CCDC-176106 for [**12**]PF_6, -176105 for [**18**]PF_6, and -176104 for [**19**]PF_6. Copies of the data can be obtained free of charge on application to CCDC, 12 Union Road, Cambridge CB2 1EZ, UK [Fax: (internat.) + 44-1223/336-033; E-mail: deposit@ccdc.cam.ac.uk].

[12]PF_6: The structure determination was hampered by the poor quality of the data caused by the inferior quality of the crystals, which was, unfortunately, the best that could be achieved. The crystal diffracted very weakly, and no reliable data could be collected at θ > 55° (resolution 0.95 Å). Moreover a more than average crystal decay was observed, up to 17%. No attempt was made to locate the hydrogen atoms attached to the disordered CH_3OH and partially occupied H_2O moieties; they cannot be calculated and no indication whatsoever of their location was found in the difference fourier map. From the anisotropic thermal displacement parameters for the PF_6 moiety it is clear that these atoms show a large positional disorder. Although it is possible to use several partially occupied positions for these atoms, no physically reasonable model results from these parameters, at least not any better than the model presented here. Because the EMPABS procedure,[17] by itself, was not adequate enough, presumably caused by the poor quality of the data and hence the ψ-scans, an additional absorption correction was applied using the DIFABS procedure.[22] Even then it was necessary to use the SIMU option in the least-squares refinement to end up with physically acceptable anisotropic thermal displacement parameters. Geometrical calculations (PLATON-93)[21] revealed neither unusual geometric features, nor unusual short intermolecular contacts. The calculations revealed no higher symmetry and no (further) solvent accessible areas.

[18]PF_6: Unfortunately the crystal structure determination was influenced by a rather severe but regular crystal decay of up to 43%. From the anisotropic thermal displacement parameters for the PF_6 moiety it is clear that these atoms show a large positional disorder. Although it is possible to use several partially occupied positions for these atoms, no physically reasonable model results from these parameters, at least not any better than the model presented here. Moreover, the model presented here was the only one that was stable by itself without the need for additional restraints. Calculations (PLATON-93)[21] showed a small void of 162 Å^3, containing at least 6 electrons, around 0,1/2,0. This electron density is assumed to be a disordered water molecule, and the SQUEEZE (PLATON-93) procedure was applied to account for this electron density. This assumption accounts for the physical molecular properties as given in Table 2.

[19]PF_6: Geometrical calculations (PLATON-93)[21] revealed neither unusual geometric features, nor unusual short intermolecular contacts. The calculations revealed no higher symmetry and no solvent accessible areas.

Syntheses

Methylbis[(6-methyl-2-pyridyl)methyl]amine (Me_2-dpa-Me): To CH_3CN (300 mL), 2-(chloromethyl)-6-methylpyridine·HCl[23] (7.98

g, 44.8 mmol), CH_3NH_2·HCl (2.27 g, 33.6 mmol), Na_2SO_4 (25.00 g), and Na_2CO_3 (47.50 g) were added. The resulting suspension was heated to reflux for 16 h. The mixture was filtered and the filtrate was concentrated yielding a brown oil, to which Et_2O (100 mL) was added. Partial evaporation of the solvent resulted in precipitation of Me_2-dpa-Me as a white solid (> 95% pure according to GC), which was crystallized as white crystals from a saturated hexane solution at −20 °C. Yield 2.52 g (16.8 mmol, 50%). An alternative synthetic route to Me_2-dpa-Me has been reported, mentioning its melting point and C,H,N analysis.[24] ^{1}H NMR (200.13 MHz, $CDCl_3$, 289 K): δ [ppm] = 7.54 (t, $^3J_{H,H}$ = 7.7 Hz, 2 H, Py-H^4), 7.34 (d, $^3J_{H,H}$ = 7.7 Hz, 2 H, Py-H^3), 7.00 (d, $^3J_{H,H}$ = 7.7 Hz, 2 H, Py-H^5), 3.74 (s, 4 H, N-*CH*$_2$-Py^{Me}), 2.54 (s, 6 H, Py-*CH*$_3$), 2.30 (s, 3 H, N-*CH*$_3$). ^{13}C{^{1}H} NMR (75.47 MHz, $CDCl_3$, 289 K): δ [ppm] = 158.6 (Py-C^2), 157.4 (Py-C^6), 136.4 (Py-C^4), 121.2 (Py-C^5), 119.6 (Py-C^3), 63.6 (N-*C*H$_2$-Py^{Me}), 42.6 (N-*C*H$_3$), 24.3 (Py-*C*H$_3$).

[(κ^4-Me$_3$-tpa)Rh^I(C$_2$H$_4$)]PF$_6$ ([11]PF$_6$): [(C$_2$H$_4$)$_2$Rh(μ-Cl)]$_2$ (270 mg, 0.69 mmol) and Me_3-tpa (375 mg, 1.13 mmol) were stirred in MeOH (55 mL) at −78 °C for about 4 h until a clear solution was obtained. Subsequently, KPF_6 (127 mg, 0.69 mmol) was added. Partial evaporation of the solvent caused the precipitation of [**11**]PF_6 as a yellow powder, which was collected by filtration and dried under vacuum. Yield 370 mg (0.61 mmol, 63%). ^{1}H NMR 200.13 MHz, CD_2Cl_2, 298 K): δ [ppm] = 7.42 (t, $^3J_{H,H}$ = 7.8 Hz, 3 H, Py^A-H^4 and Py^B-H^4), 7.16 (d, $^3J_{H,H}$ = 7.3 Hz, 1 H, Py^B-H^3 or Py^B-H^5), 7.04 (d, $^3J_{H,H}$ = 7.6 Hz, 2 H, Py^A-H^3 or Py^B-H^5), 6.89 (d, $^3J_{H,H}$ = 7.6 Hz, 3 H, Py^B-H^3 or -H^5 or Py^A-H^3 or -H^5), 5.63 (d[AB], $^2J_{H,H}$ = 15.3 Hz, 2 H, N-*CH*$_2$-Py^A), 4.80 (d[AB], $^2J_{H,H}$ = 15.3 Hz, 2 H, N-*CH*$_2$-Py^A), 4.41 (s, 2 H, N-*CH*$_2$-Py^B), 3.71 (s, 3 H, Py^B-*CH*$_3$), 2.87 (s, 6 H, Py^A-*CH*$_3$), 2.54−2.34 (m, 2 H, *CH*$_2$=CH$_2$), 2.25−2.05 (m, 2 H, CH$_2$=*CH*$_2$). ^{13}C{^{1}H} NMR (50.32 MHz, CD_2Cl_2, 289 K): δ [ppm] = 163.8 (Py^B-C^2), 163.6 (Py^A-C^2), 161.0 (Py^B-C^6), 159.6 (Py^A-C^6), 138.0 (Py^B-C^4), 137.8 (Py^A-C^4), 125.5 (Py^A-C^3), 124.5 (Py^B-C^3), 120.5 (Py^A-C^5), 119.9 (Py^B-C^5), 70.5 (N-*C*H$_2$-Py^A), 63.7 (N-*C*H$_2$-Py^B), 31.7 (Py^B-*C*H$_3$), 29.5 (d, $^1J_{Rh,H}$ = 16.9 Hz, *CH*$_2$=CH$_2$), 28.2 (Py^A-*C*H$_3$), 26.3 (d, $^1J_{Rh,H}$ = 19.9 Hz, CH$_2$=*CH*$_2$). FAB$^+$-MS: *m*/*z* = 463 [M − PF$_6$]$^+$. $C_{23}H_{28}F_6N_4PRh$ (608.37): calcd. C 45.41, H 4.64, N 9.21; found C 45.18, H 4.71, N 9.40.

[(κ^3-Me$_3$-tpa)Ir^I(C$_2$H$_4$)$_2$]PF$_6$ ([12]PF$_6$): [Ir(coe)$_2$Cl)$_2$ (350 mg, 0.39 mmol) was dissolved in methanol (14 mL). Ethene was bubbled through the solution until a clear solution was obtained. The solution was cooled to −30 °C and Me_3-tpa (260 mg, 0.78 mmol) was added under ethene. The reaction mixture was stirred until the Me_3-tpa had dissolved. Subsequently, KPF_6 (170 mg, 0.92 mmol) was added and the solution was stirred for 1 h at −30 °C, after which the solution was cooled to −78 °C causing the precipitation of [**12**]PF_6. A second portion was obtained by adding KPF_6 (25 mg, 0.14 mmol) to the filtrate, stirring for 1 h at −50 °C, and leaving overnight at −20 °C. The yellow solid thus obtained was collected by filtration, washed three times with cold methanol (−78 °C) under nitrogen and dried under vacuum. Yield: 311 mg (0.43 mmol, 55%). ^{1}H NMR (200.13 MHz, CD_2Cl_2, 289 K): δ [ppm] = 7.80 (t, $^3J_{H,H}$ = 7.7 Hz, 1 H, Py^B-H^4), 7.71 (t, $^3J_{H,H}$ = 7.7 Hz, 2 H, Py^A-H^4), 7.38 (d, $^3J_{H,H}$ = 7.7 Hz, 2 H, Py$^{A/B}$-H$^{3/5}$), 7.34 (d, $^3J_{H,H}$ = 7.7 Hz, 2 H, Py$^{A/B}$-H$^{3/5}$), 7.24 (d, $^3J_{H,H}$ = 7.7 Hz, 2 H, Py$^{A/B}$-H$^{3/5}$), 5.26 (d[AB], $^2J_{H,H}$ = 16.0 Hz, 2 H, N-*CH*$_2$-Py^A), 4.94 (s, 2 H, N-*CH*$_2$-Py^B), 3.92 (d[AB], $^2J_{H,H}$ = 16.0 Hz, 2 H, N-*CH*$_2$-Py^A), 3.28 (s, 6 H, CH$_3$-Py^A). 2.62 (s, 3 H, CH$_3$-Py^B), 2.02 (br, 4 H, CH$_2$=CH$_2$), 1.81 (br, 4 H, CH$_2$=CH$_2$). $C_{25}H_{32}F_6IrN_4P$ (725.74): calcd. C 41.38, H 4.44, N 7.72, found C 41.19, H 4.20, N 7.80.

[(κ^3-Me$_2$-dpa-Me)Ir^I(C$_2$H$_4$)$_2$]PF$_6$ ([13]PF$_6$): [Ir(coe)$_2$Cl]$_2$ (350 mg, 0.39 mmol) was dissolved in methanol (14 mL), ethene was bubbled through the solution until a clear solution was obtained. The solution was cooled to −30 °C and Me_2-dpa-Me (190 mg, 0.79 mmol) was added under ethene. The reaction mixture was stirred until the Me_2-dpa-Me had dissolved. Subsequently, KPF_6 (170 mg, 0.92 mmol) was added and the solution was stirred for 1 h at −30 °C, after which the solution was cooled to −78 °C causing precipitation of [**13**]PF_6. A second portion was obtained by adding KPF_6 (25 mg, 0.14 mmol) to the filtrate, stirring for 1 h at −50 °C, and leaving overnight at −20 °C. The resulting yellow solid was collected by filtration, washed three times with cold methanol (−78 °C) under nitrogen and dried under vacuum. Yield: 234 mg (0.37 mmol, 47%). ^{1}H NMR (200.13 MHz, CD_3CN, 289 K): δ [ppm] = 7.73 (t, $^3J_{H,H}$ = 7.7 Hz, 2 H, Py-H^4), 7.37 (d, $^3J_{H,H}$ = 7.7 Hz, 2 H, Py-H$^{3/5}$), 7.27 (d, $^3J_{H,H}$ = 7.7 Hz, 2 H, Py-H$^{3/5}$), 4.64 (d[AB], $^2J_{H,H}$ = 15.8 Hz, 2 H, CH$_2$-Py), 4.10 (d[AB], $^2J_{H,H}$ = 15.8 Hz, 2 H, CH$_2$-Py), 3.34 (s, 3 H, CH$_3$-N), 3.18 (s, 6 H, CH$_3$-Py), 1.83 (br, 4 H, CH$_2$=CH$_2$), 1.67 (br, 4 H, CH$_2$=CH$_2$). $C_{19}H_{27}F_6IrN_3P$ (634.63): calcd. C 35.96, H 4.29, N 6.62; found C 35.66, H 4.10, N 6.39.

[(κ^4-Me$_3$-tpa)Ir^I(C$_2$H$_4$)]PF$_6$ ([14]PF$_6$): Compound [**12**]PF_6 (100 mg, 0.14 mmol) was dissolved in acetone (5 mL) and stirred for 4 h under nitrogen at room temp. The gas phase was flushed with fresh nitrogen every hour. Subsequently, 25 mL of hexane was added causing precipitation of [**14**]PF_6. The resulting orange solid was collected by filtration, washed 3 times with cold hexane and dried under vacuum. Yield 42 mg (0.07 mmol, 50%). ^{1}H NMR (200.13 MHz, CD_3CN, 289 K): δ [ppm] = 7.54 (t, $^3J_{H,H}$ = 7.7 Hz, 1 H, Py^B-H^4), 7.50 (t, $^3J_{H,H}$ = 7.7 Hz, 2 H, Py^A-H^4), 7.24 (d, $^3J_{H,H}$ = 7.7 Hz, 2 H, Py^A-H^3/Py^B-H$^{3\&5}$), 7.09 (d, $^3J_{H,H}$ = 7.7 Hz, 2 H, Py^A-H$^{5/3}$/Py^B-H$^{3\&5}$), 7.02 (d, $^3J_{H,H}$ = 7.7 Hz, 2 H, Py^A-H^5/Py^B-H$^{3\&5}$), 5.29 (d[AB], $^2J_{H,H}$ = 15.3 Hz, N-*CH*$_2$-Py^A), 4.85 (d[AB], $^2J_{H,H}$ = 15.3 Hz N-*CH*$_2$-Py^A), 4.64 (s, N-*CH*$_2$-Py^B), 3.65 (s, 3 H, Py^B-CH$_3$), 2.85 (s, 6 H, Py^A-CH$_3$), 1.85 (t, 2 H, $^3J_{H,H}$ = 8.6 Hz, *CH*$_2$=CH$_2$), 1.37 (t, 2 H, $^3J_{H,H}$ = 8.58 Hz, CH$_2$=*CH*$_2$). ^{1}H NMR (400.14 MHz, [D$_6$]acetone, 289 K): δ [ppm] = 7.72 (t, $^3J_{H,H}$ = 7.8 Hz, 1 H, Py^B-H^4), 7.60 (t, $^3J_{H,H}$ = 7.8 Hz, 2 H, Py^A-H^4), 7.35 (d, $^3J_{H,H}$ = 7.2 Hz, 1 H, Py^B-H^3), 7.26 (d, $^3J_{H,H}$ = 7.6 Hz, 2 H, Py^A-H^3), 7.15 (d, $^3J_{H,H}$ = 7.3 Hz, 1 H, Py^B-H^5), 7.81 (d, $^3J_{H,H}$ = 7.8 Hz, 2 H, Py^A-H^5), 5.49 (d[AB], $^2J_{H,H}$ = 15.2 Hz, N-*CH*$_2$-Py^A), 5.11 (d[AB], $^2J_{H,H}$ = 15.2 Hz, N-*CH*$_2$-Py^A), 4.90 (s, N-*CH*$_2$-Py^B), 3.75 (s, 3 H, Py^B-*CH*$_3$), 2.94 (s, 6 H, Py^A-*CH*$_3$), 1.89 (t, 2 H, $^3J_{H,H}$ = 8.6 Hz, *CH*$_2$=CH$_2$), 1.47 (t, 2 H, $^3J_{H,H}$ = 8.79 Hz, CH$_2$=*CH*$_2$). ^{13}C{^{1}H} NMR (100.61 MHz, [D$_6$]acetone, 289 K): δ [ppm] = 164.6 (Py^A-C^6), 163.2 (Py^A-C^2), 161.8 (Py^B-C^6), 160.2 (Py^B-C^2), 138.4 (Py^B-C^4), 136.9 (Py^A-C^4), 124.7 (Py^A-C^5), 123.5 (Py^B-C^5), 119.8 (Py^A-C^3), 118.9 (Py^B-C^3), 71.7 (N-*C*H$_2$-Py^A), 65.2 (N-*C*H$_2$-Py^B), 32.5 (Py^B-*C*H$_3$), 27.2 (Py^A-*C*H$_3$), 3.7 (*C*H$_2$=CH$_2$), 0.2 (CH$_2$=*C*H$_2$). ESI$^+$-MS: *m*/*z* = 553 [M − PF$_6$]$^+$. $C_{23}H_{28}F_6IrN_4P$ (697.69): calcd. C 39.60, H 4.04, N 8.03; found C 39.43, H 4.17, N 8.20.

[(κ^3-Me$_2$-dpa-Me)Ir^I(C$_2$H$_4$)]PF$_6$ ([15]PF$_6$): Dissolving [**13**]PF_6 in CD_2Cl_2 resulted in the formation of [**15**]PF_6 within 2 h. ^{1}H NMR (200.13 MHz, CD_2Cl_2, 289 K): δ [ppm] = 7.59 (t, $^3J_{H,H}$ = 7.7 Hz, 2 H, Py-H^4), 7.17 (d, $^3J_{H,H}$ = 7.5 Hz, 2 H, Py-H^3), 7.05 (d, $^3J_{H,H}$ = 7.9 Hz, 2 H, Py-H^5), 5.07 (d[AB], $^2J_{H,H}$ = 14.9 Hz, N-*CH*$_2$-Py), 4.75 (d[AB], $^2J_{H,H}$ = 14.9 Hz, N-*CH*$_2$-Py), 3.59 (t, $^3J_{H,H}$ = 9.7 Hz, 2 H, *CH*$_2$=CH$_2$), 3.15 (s, 3 H, N-CH$_3$), 2.66 (s, 6 H, Py-CH$_3$), 2.36 (t, $^3J_{H,H}$ = 9.7 Hz, 2 H, CH$_2$=*CH*$_2$). ^{1}H NMR (400.14 MHz, CD_3CN, 289 K): δ [ppm] = 7.63 (t, $^3J_{H,H}$ = 7.9 Hz, 2 H, Py-H^4), 7.18 (d, $^3J_{H,H}$ = 7.4 Hz, 2 H, Py-H^3), 7.11 (d, $^3J_{H,H}$ = 7.9 Hz, 2

H, Py-H^5), 5.06 (d[AB], $^2J_{H,H}$ = 15.1 Hz, N-*CH*$_2$-Py), 4.71 (d[AB], $^2J_{H,H}$ = 15.1 Hz, N-*CH*$_2$-Py), 3.54 (t, $^3J_{H,H}$ = 9.7 Hz, 2 H, *CH*$_2$=CH$_2$), 3.11 (s, 3 H, N-CH$_3$), 2.64 (s, 6 H, Py-CH$_3$), 2.34 (t, $^3J_{H,H}$ = 9.7 Hz, 2 H, CH$_2$=*CH*$_2$). ^{13}C{^{1}H} NMR (75.47 MHz, CD$_3$CN, 289 K): δ [ppm] = 166.6 (Py-C^6), 164.4 (Py-C^2), 138.7 (Py-C^4), 127.2 (Py-C^5), 121.9 (Py-C^3), 72.2 (N-*C*H$_2$-Py), 52.4 (N-*C*H$_3$), 37.0 (*C*H$_2$=CH$_2$), 27.1 (Py-*C*H$_3$), 25.1 (CH$_2$=*C*H$_2$). Due to the instability of [**15**]PF$_6$, reliable elemental analytical data were not obtained.

[(κ^3-Me$_2$-dpa-Me)Ir^{I}(C$_2$H$_4$)]PF$_6$ ([15(MeCN)]PF$_6$): Dissolving [**13**]PF$_6$ in CD$_3$CN resulted in a 3:1 mixture of [**15**]PF$_6$ and [**15**(MeCN)]PF$_6$ within 2 h. ^{1}H NMR (400.14 MHz, CD$_3$CN, 289 K): δ [ppm] = 7.63 (t, $^3J_{H,H}$ = 7.8 Hz, 2 H, Py-H^4), 7.20 (d, $^3J_{H,H}$ = 7.9 Hz, 2 H, Py-H^3), 7.16 (d, $^3J_{H,H}$ = 7.8 Hz, 2 H, Py-H^5), 4.95 (d[AB], $^2J_{H,H}$ = 14.9 Hz, N-*CH*$_2$-Py), 4.57 (d[AB], $^2J_{H,H}$ = 14.9 Hz, N-*CH*$_2$-Py), 2.91 (s, 6 H, Py-CH$_3$), 2.78 (s, 3 H, N-CH$_3$), 1.94 (t, $^3J_{H,H}$ = 8.7 Hz, 2 H, *CH*$_2$=CH$_2$), 1.28 (t, $^3J_{H,H}$ = 8.7 Hz, 2 H, CH$_2$=*CH*$_2$). ^{13}C{^{1}H} NMR (75.47 MHz, CD$_3$CN, 289 K): δ [ppm] = 166 (Py-C^6), 164 (Py-C^2), 137.0 (Py-C^4), 127.2 (Py-C^5), 120.0 (Py-C^3), 72.6 (N-*C*H$_2$-Py), 51.4 (N-*C*H$_3$), 27.6 (Py-*C*H$_3$). ^{13}C NMR signals of the ethene fragment could not be observed at 289 K. Due to the instability of [**15**(MeCN)]PF$_6$, reliable elemental analytical data were not obtained.

[(κ^4-C,*N*,*N*′,*N*′′-Me$_3$-tpa)Ir(H)(CD$_3$CN)]PF$_6$ ([16]PF$_6$): Compound [**14**]PF$_6$ (20 mg, 0.03 mmol) was dissolved in MeCN (1 mL) and was kept for 3 d under nitrogen. Sample prepared in CD$_3$CN: CPy represents the unique cyclometallated pyridyl group (at C^3). ^{1}H NMR (500 MHz, CD$_3$CN, 289 K): δ [ppm] = 7.81 (d, $^3J_{H,H}$ = 7.7 Hz, CPy-H^5), 7.63 (t, $^3J_{H,H}$ = 7.7 Hz, 2 H, Py^A-H^4), 7.25 (d, $^3J_{H,H}$ = 7.2 Hz, 2 H, Py^A-H^3), 7.23 (d, $^3J_{H,H}$ = 7.7 Hz, 2 H, Py^A-H^5), 6.48 (d, $^3J_{H,H}$ = 7.7 Hz, CPy-H^4), 5.09 (d[AB], $^2J_{H,H}$ = 15.3 Hz, 2 H, N-*CH*$_2$-Py^A), 5.04 (d[AB], $^2J_{H,H}$ = 15.3 Hz, 2 H, N-*CH*$_2$-Py^A), 4.41 (s, 2 H, N-*CH*$_2$-CPy), 2.81 (s, 6 H, Py^A-CH$_3$), 2.13 (s, 3 H, CPy-CH$_3$), −18.58 (s, Ir-H). ^{13}C{^{1}H} NMR (75.47 MHz, CD$_3$CN, 289 K): δ [ppm] = 169.6 (CPy-C^6), 167.0 (Py^A-C^6), 164.6 (CPy-C^2), 151.8 (CPy-C^5), 151.2 (Py^A-C^2), 139.0 (Py^A-C^4), 127.3 (CPy-C^3-Ir), 124.9 (Py^A-C^5), 121.9 (CPy-C^4), 121.7 (Py^A-C^3), 70.4 (N-*C*H$_2$-Py^A), 68.8 (N-*C*H$_2$-CPy), 31.6 (*C*H$_3$-Py^A), 23.2 (*C*H$_3$-CPy). ESI-MS: *m*/*z* = 569 [M − PF$_6$]$^+$. Sample prepared in CH$_3$CN: ESI-MS: *m*/*z* = 566 [M − PF$_6$]$^+$. C$_{23}$H$_{27}$F$_6$IrN$_5$P (710.68): calcd. C 38.87, H 3.83, N 9.85; found C 39.07, H 4.01, N 9.99.

[(κ^4-C,*N*,*N*′,*N*′′-Me$_3$TPA)Ir(H)(C$_2$H$_4$)](PF$_6$): [**14**]PF$_6$ (10 mg, 0.015 mmol) was dissolved in CD$_2$Cl$_2$ (1 mL) and kept for 3 d under nitrogen. ^{1}H NMR: (200 MHz, CD$_2$Cl$_2$): δ [ppm] = 8.23 (d, CPy-H^5, $^3J_{H,H}$ = 7.4 Hz), 7.58 (t, 2 H, Py^A-H^4, $^3J_{H,H}$ = 7.9 Hz), 7.22 (d, 2 H, CPy-H^3, $^3J_{H,H}$ = 7.7 Hz), 7.13 (d, 2 H, Py^A-H^5, $^3J_{H,H}$ = 7.7 Hz), 6.70 (d, CPy-H^4, $^3J_{H,H}$ = 7.7 Hz), 5.50 (d[AB], N-*CH*$_2$-Py^A, $^2J_{H,H}$ = 16.0 Hz), 5.27 (d[AB], N-*CH*$_2$-Py^A, $^2J_{H,H}$ = 16.0 Hz), 4.68 (s, 2 H, N-*CH*$_2$-CPy), 3.53 (s, 4 H, *CH*$_2$=*CH*$_2$), 2.75 (s, 6 H, Py^A-*CH*$_3$), 2.22 (s, 3 H, CPy-*CH*$_3$), -15.87 (s, Ir-*H*).

[(k^4-Me$_3$-tpa)Rh^{III}(O$_2$)]PF$_6$ ([17]PF$_6$): A solution of [**11**]PF$_6$ (50 mg, 0.082 mmol) in CH$_2$Cl$_2$ (2 mL) was vigorously stirred at room temperature in contact with O$_2$ for about 30 min. The peroxo complex **17** was formed in 100% yield. Addition of hexane to the solution caused precipitation of [**17**]PF$_6$ as a light-brown solid, which was collected by filtration and dried under vacuum. ^{1}H NMR (200.13 MHz, CD$_2$Cl$_2$, 298 K): δ [ppm] = 7.63 (t, $^3J_{H,H}$ = 7.7 Hz, 2 H, Py^A-H^4), 7.60 (t, $^3J_{H,H}$ = 7.7 Hz, 1 H, Py^B-H^4), 7.34 (d, $^3J_{H,H}$ = 7.6 Hz, 1 H, Py^B-H^3 or -H^5), 7.24 (d, $^3J_{H,H}$ = 7.6 Hz, 2 H, Py^A-H^3 or -H^5), 7.11 (d, $^3J_{H,H}$ = 7.8 Hz, 1 H, Py^B-H^3 or -H^5), 7.10 (d, $^3J_{H,H}$ = 8.1 Hz, 2 H, Py^A-H^3 or -H^5), 5.64 (d[AB], $^2J_{H,H}$ = 15.5 Hz, 2 H, N-C*H*$_2$-Py^A), 5.15 (d[AB], $^2J_{H,H}$ = 15.5 Hz, 2 H, N-C*H*$_2$-Py^A), 4.68 (s, 2 H, N-C*H*$_2$-Py^B), 3.56 (s, 3 H, Py^B-C*H*$_3$), 3.03 (s, 6 H, Py^A-C*H*$_3$). ^{13}C{^{1}H} NMR (50.31 MHz, CD$_2$Cl$_2$, 298 K): δ [ppm] = 165.4, 162.7, 162.6, 160.3 (Py^B- and Py^A-C^2, Py^B- and Py^A-C^6), 139.8 (Py^A-C^4), 139.5 (Py^B-C^4), 127.6 (Py^A-C^3), 126.3 (Py^B-C^3), 120.8 (Py^A-C^5), 119.9 (Py^B-C^5), 72.0 (N-*C*H$_2$-Py^A), 67.5 (N-*C*H$_2$-Py^B), 31.3 (Py^B-*C*H$_3$), 24.2 (Py^A-*C*H$_3$). FAB$^+$-MS: *m*/*z* = 467 [M − PF$_6$]$^+$: *m*/*z* = 1079 [2 M − PF$_6$]$^+$. ESI-MS with argon as a collision gas: *m*/*z* = 467 [M − PF$_6$]$^+$. C$_{21}$H$_{24}$F$_6$N$_4$O$_2$PRh (612.32): calcd. C 41.19, H 3.95, N 9.15; found C 40.29, H 4.72, N 8.46.

[(κ^3-Me$_3$-tpa)Ir^{III}(C$_2$H$_4$)(O$_2$)]PF$_6$ ([18]PF$_6$): Compound [**14**]PF$_6$ (40 mg, 0.06 mmol) was dissolved in dichloromethane (4 mL) and placed under 1.6 bar of O$_2$ for 30 min. The solution was filtered and dried under vacuum. Yellow/brown crystals of [**18**]PF$_6$, suitable for X-ray diffraction, were obtained by vapor-vapor diffusion of diethyl ether and a solution of [**18**]PF$_6$ in MeCN. A separate volumetric gas-uptake measurement indicated consumption of 1 mol of O$_2$ per mol of [**14**]PF$_6$. During this reaction [**14**]PF$_6$ (150 mg, 0.15 mmol) consumed ca. 3.40 mL of O$_2$ (0.14 mmol). Isolated yield 7.3 mg (0.01 mmol, 16%). ^{1}H NMR (400.14 MHz, [D$_6$]acetone, 289 K): δ [ppm] = 7.97 (t, $^3J_{H,H}$ = 7.8 Hz, 2 H, Py^A-H^4), 7.82 (t, $^3J_{H,H}$ = 7.6 Hz, 1 H, Py^B-H^4), 7.63 (d, $^3J_{H,H}$ = 7.8 Hz, 2 H, Py^A-H^3), 7.43 (d, $^3J_{H,H}$ = 7.4 Hz, 1 H, Py^B-H^5), 7.41 (d, $^3J_{H,H}$ = 7.8 Hz, 2 H, Py^A-H^5), 7.37 (d, $^3J_{H,H}$ = 7.6 Hz, 1 H, Py^B-H^3), 5.79 (d[AB], $^3J_{H,H}$ = 16.0 Hz, 2 H, Py^A-*CH*$_2$-N), 5.05 (d[AB], $^3J_{H,H}$ = 16.0 Hz, 2 H, Py^A-*CH*$_2$-N), 4.80 (s, 2 H, Py^B-*CH*$_2$-N), 4.48 (br, 4 H, *CH*$_2$=*CH*$_2$), 2.96 (s, 6 H, Py^A-CH$_3$), 2.65 (s, 3 H, Py^B-CH$_3$). ^{13}C{^{1}H} NMR (75.47 MHz, [D$_6$]acetone, 289 K): δ (ppm) = 166 (Py^A-C^2), 166 (Py^A-C^2), 165 (Py^A-C^6), 159.5 (Py^B-C^6), 151 (Py^B-C^2), 140.2 (Py^A-C^4), 137.9 (Py^B-C^4), 128 (Py^A-C^5), 124.5 (Py^B-C^3), 124 (Py^B-C^5), 122 (Py^A-C^3), 65.5 (N-*C*H$_2$-Py^A), 62.7 (N-*C*H$_2$-Py^B), 22.0 (Py^A-*C*H$_3$ & Py^B-*C*H$_3$). ^{13}C NMR signals of the ethene fragment could not be observed at 289 K. ESI-MS: 585 [M − PF$_6$]$^+$, 557 [M − PF$_6$ − C$_2$H$_4$]$^+$, 553 [M − PF$_6$ − O$_2$]$^+$, 566 [M − PF$_6$ − O$_2$ − C$_2$H$_4$ + CH$_3$CN]$^+$. C$_{23}$H$_{28}$F$_6$IrN$_4$O$_2$P (729.68): calcd. C 37.86, H 3.87, N 7.68; found C 38.05, H 4.03, N 7.85.

[(κ^3-Me$_2$-dpa-Me)Ir^{III}(C$_2$H$_4$)(O$_2$)]PF$_6$ ([19]PF$_6$): [**15**]PF$_6$ (40 mg, 0.112 mmol) was dissolved in 4 mL of dichloromethane and placed under of 1.6 bar of O$_2$ for 30 min. The solution was filtered and dried under vacuum. Light-brown crystals of [**19**]PF$_6$, suitable for X-ray diffraction, were obtained by vapor-vapor diffusion of hexane and a solution of [**19**]PF$_6$ in acetone. Isolated yield 7.7 mg (0.012 mmol, 16%). ^{1}H NMR (400.14 MHz, CD$_3$CN, 289 K): δ [ppm] = 7.78 (t, $^3J_{H,H}$ = 7.8 Hz, 2 H, Py-H^4), 7.35 (d, $^3J_{H,H}$ = 7.8 Hz, 1 H, Py-H^3), 7.22 (d, $^3J_{H,H}$ = 8.1 Hz, 2 H, Py-H^5), 4.93 (d[AB], $^2J_{H,H}$ = 15.6 Hz, 2 H, N-*CH*$_2$-Py), 4.86 (d[AB], $^2J_{H,H}$ = 15.6 Hz, 2 H, N-*CH*$_2$-Py), 4.22 (br, 4 H, C$_2$H$_4$), 3.23 (s, 3 H, N-CH$_3$), 2.82 (s, 6 H, Py-CH$_3$). ^{1}H NMR (400.14 MHz, [D$_6$]acetone, 289 K): δ [ppm] = 7.93 (t, $^3J_{H,H}$ = 7.8 Hz, 2 H, Py-H^4), 7.56 (d, $^3J_{H,H}$ = 7.8 Hz, 1 H, Py-H^3), 7.37 (d, $^3J_{H,H}$ = 7.8 Hz, 2 H, Py-H^5), 5.53 (d[AB], $^2J_{H,H}$ = 15.6 Hz, 2 H, N-*CH*$_2$-Py), 5.21 (d[AB], $^2J_{H,H}$ = 15.6 Hz, 2 H, N-*CH*$_2$-Py), 4.36 (br, 4 H, *CH*$_2$=*CH*$_2$), 3.41 (s, 3 H, N-*CH*$_3$), 2.92 (s, 6 H, Py-*CH*$_3$). ^{13}C{^{1}H} NMR (75.47 MHz, CD$_3$CN, 289 K): δ [ppm] = 166.1 (Py-C^2), 165.5 (Py-C^6), 140.7 (Py-C^4), 128.6 (Py-C^5), 122.5 (Py-C^3), 71.3 (N-*C*H$_2$-Py), 52.7 (N-*C*H$_3$), 23.0 (Py-*C*H$_3$). ^{13}C NMR signals of the ethene fragment could not be observed at 289 K. C$_{17}$H$_{23}$F$_6$IrN$_3$O$_2$P (638.57): calcd. C 31.98, H 3.63, N 6.58; found C 32.14, H 3.61, N 6.38.

[1] [1a] H. Mimoun, *Pure Appl. Chem.* **1981**, *53*, 2389. [1b] F. Di Furia, G. Modena, *Pure Appl. Chem.* **1982**, *54*, 1853. [1c] O.

Bortolini, F. Di Furia, G. Modena, R. Seraglia, *J. Mol. Catal.* **1984**, *22*, 313. [1d] K. Takao, Y. Fujiwara, T. Imanaka, S. Teranishi, *Bull. Chem. Soc. Jpn.* **1970**, *43*, 1153. [1e] K. Takao, M. Wayaku, Y. Fujiwara, T. Imanaka, S. Teranishi, *Bull. Chem. Soc. Jpn.* **1970**, *43*, 3898. [1f] C. Dudley, G. Read, *Tetrahedron Lett.* **1972**, 5273. [1g] G. Read, P. J. C. Walker, *J. Chem. Soc., Dalton Trans.* **1977**, 883. [1h] L. Carlton, G. Read, M. Urgelles, *J. Chem. Soc., Chem. Commun.* **1983**, 586. [1i] G. Read, M. Urgelles, *J. Chem. Soc., Dalton Trans.* **1985**, 1591. [1j] H. Mimoun, M. M. P. Machirant, I. S. de Roch, *J. Am. Chem. Soc.* **1978**, *100*, 5437. [1k] F. Igersheim, H. Mimoun, *Nouv. J. Chim.* **1980**, *4*, 161.

[2] G. Strukul, R. A. Michelin, *J. Am. Chem. Soc.* **1985**, *107*, 7563.

[3] G. Read, *J. Mol. Catal.* **1988**, *44*, 15.

[4] [4a] K. A. Jørgensen, *Chem. Rev.* **1989**, *89*, 431. [4b] K. A. Jørgensen, B. Schiøtt, *Chem. Rev.* **1990**, *90*, 1483.

[5] [5a] B. de Bruin, M. J. Boerakker, J. J. J. M. Donners, B. E. C. Christiaans, P. P. J. Schlebos, R. de Gelder, J. M. M. Smits, A. L. Spek, A. W. Gal, *Angew. Chem. Int. Ed. Engl.* **1997**, *36*, 2064; *Angew. Chem.* **1997**, *109*, 2153. [5b] B. de Bruin, M. J. Boerakker, R. de Gelder, J. M. M. Smits, A. W. Gal, *Angew. Chem. Int. Ed.* **1999**, *38*, 219; *Angew. Chem.* **1999**, *111*.118. [5c] B. de Bruin, M. J. Boerakker, J. A. W. Verhagen, R. de Gelder, J. M. M. Smits, A. W. Gal, *Chem. Eur. J.* **2000**, *6*, 298. [5d] B. de Bruin, J. A. Brands, J. J. J. M. Donners, M. P. J. Donners, R. de Gelder, J. M. M. Smits, A. L. Spek, A. W. Gal, *Chem. Eur. J.* **1999**, *5*, 2921.

[6] R. J. N. A. M. Kicken, Thesis ("Oxidation of Iridium Olefin Complexes by H_2O_2 and O_2"), University of Nijmegen, **2001**.

[7] M. Krom, R. G. E. Coumans, J. M. M. Smits, A. W. Gal, *Angew. Chem. Int. Ed. Eng.* **2001**, *40*, 2106−2108, *Angew. Chem.* **2001**, *113*, 2164−2166.

[8] M. Krom, T. P. J. Peters, A. W. Gal, to be published.

[9] A. L. Onderlinden, A. van der Ent, *Inorg. Chim. Acta* **1972**, *6*, 420−426.

[10] J. L. Herde, J. C. Lambert, C. V. Senoff, *Inorg. Synth.* **1974**, *15*, 18−20.

[11] R. Hoffmann, J. Saillard, *J. Am. Chem. Soc.* **1984**, *106*, 2006−2026.

[12] A. Vigalok, L. J. W. Shimon, D. Milstein, *Chem. Commun.* **1996**, 1673.

[13] This kind of reactivity (path **d**) has been observed for (ethene)Ir^{I} (see ref.[6]) and (cod)Rh^{I} complexes (see ref.[5d]).

[14] See also: R. Jiménez-Cantaño, S. Niu, M. B. Hall, *Organometallics* **1997**, 1962−1968.

[15] H. Nagao, N. Komeda, M. Mukaida, M. Suzuki, K. Tanaka, *Inorg. Chem.* **1996**, *35*, 6809−6815.

[16] R. Cramer, J. A. McCleverty, J. Bray, *Inorg. Synth.* **1990**, *28*, 86.

[17] A. C. T. North, D. C. Phillips, F. C. Mathews, *Acta Crystallogr., Sect. A* **1968**, *24*, 351.

[18] P. T. Beurskens, G. Beurskens, W. P. Bosman, R. de Gelder, S. Garcia-Granda, R. O. Gould, R. Israel, J. M. M. Smits, *DIRDIF-96, A computer program system for crystal structure determination by Patterson methods and direct methods applied to difference structure factors*, Laboratory of Crystallography, Department of Inorganic Chemistry, University of Nijmegen, The Netherlands, **1996**.

[19] P. T. Beurskens, G. Beurskens, M. Strumpel, C. E. Nordman, in: *Patterson and Pattersons* (Eds.: J. P. Glusker, B. K. Patterson, M. Rossi), Clarendon Press, Oxford, **1987**, p. 356.

[20] G. M. Sheldrick, *SHELXL-97, Program for the refinement of crystal structures*, University of Göttingen, Germany, **1997**.

[21] A. L. Spek, *PLATON-93*, *Program for display and analysis of crystal and molecular structures*, University of Utrecht, The Netherlands, **1995**.

[22] N. Walker, D. Stuart, *Acta Crystallogr., Sect. A* **1983**, *39*, 158.

[23] W. Baker, K. M. Bugg, J. F. McOmie, D. A. Watkins, *J. Chem. Soc.* **1958**, 3595.

[24] M. M. da Mota, J. Rodgers, S. M. Nelson, *J. Chem. Soc. A* **1969**, 2036−2044.